Carbon 127 (2018) 218–227

Contents lists available at ScienceDirect

Carbon

journal homepage: www.elsevier.com/locate/carbon

Robust, hydrophilic graphene/cellulose nanocrystal fiber-based electrode with high capacitive performance and conductivity

Guoyin Chen, Tao Chen, Kai Hou, Wujun Ma, Mike Tebyetekerwa, Yanhua Cheng, Wei Weng, Meifang Zhu*

State Key Laboratory for Modification of Chemical Fibers and Polymer Materials, College of Materials Science and Engineering, Donghua University, 2999 North Renmin Road, Shanghai 201620, People's Republic of China

ARTICLE INFO

Article history:
Received 9 August 2017
Received in revised form
20 October 2017
Accepted 4 November 2017
Available online 6 November 2017

ABSTRACT

Graphene fiber-based electrodes for supercapacitors are promising candidates for wearable energy storage. Their main limitation, although, is the low electrochemical performance caused by the restacking of graphene sheets and their hydrophobicity to electrolytes. Incorporation of nanofillers into graphene is an efficient way to overcome the challenges, however, often leading to a severe deterioration in their mechanical property and/or conductivity, thus significantly influences the practical applications and rate performance of the device. Herein, an approach of fabricating hybrid fibers from graphene oxide (GO) and cellulose nanocrystal (CNC) via non-liquid-crystal spinning and followed by chemical reduction is presented to collectively work around the problems. The resultant hybrid GO/CNC fibers demonstrated a high capacitive performance, enhanced mechanical property, and improved hydrophilicity simultaneously. Furthermore, the conductivity kept at a high value. Sample with a GO/CNC weight ratio of 100/20 possessed a high capacitance of 208.2 F cm^{-3}, a strength of 199.8 MPa, a contact angle of 63.3°, and conductivity of 64.7 S cm^{-1}. Moreover, the supercapacitor assembled from this fiber exhibited a high energy density and power density (5.1 mW h cm^{-3} and 496.4 mW cm^{-3}), excellent flexibility and bending stability, which has a great potential for use as a flexible power storage.

1. Introduction

The rapid development on miniaturization and light-weighting of wearable electronics require energy storage with more appropriate properties, such as high power density and flexibility [1–3]. Supercapacitors have advantages of high power density, fast charge/discharge rate, long lifetime, that make them attract extensive attentions in the field of wearable electronics [2,4,5]. However, there remain lots of challenges to fabricate flexible supercapacitors with high electrochemical performance [2]. In this regard, graphene-based fibers exhibit excellent flexibility, electrical property and relative high capacitive performance due to the linear fibrous structure, graphene's inherent high electrical conductivity and ultrahigh specific surface area [5–8]. Furthermore, considering the abundant resource of natural graphite and the established spinning technique, graphene-based fiber spun from graphene oxide (GO) and followed by reduction is becoming one of the most promising and suitable candidate for serving as flexible electrodes [9–13].

However, as for graphene fibers, the π-π stacking and natural hydrophobicity of graphene sheets are known to cause low specific surface area and poor compatibility with electrolyte, thus leading to a poor electrochemical property [12–15]. Up to now, many efforts have been devoted to solve these problems, which aim to fabricate graphene-based fiber with a porous structure and well hydrophilicity [16,17]. In our previous works, we successfully developed a novel method to prepare porous graphene fibers via non-liquid-crystal spinning [12,17], and proved that the highly porous structure could enhance the capacitive performance of graphene fibers due to the high specific surface area. Another stratagem is to fabricate graphene-based hybrid fibers. For instance, inorganic nanoparticles such as MnO_2 [14], MoO_3 [18], and carbon nanotube (CNT) [1,19] can be used as efficient spacers to prevent π-π stacking of graphene sheets, and the results

* Corresponding author.
E-mail address: zhumf@dhu.edu.cn (M. Zhu).

https://doi.org/10.1016/j.carbon.2017.11.012
0008-6223/

showed that their capacitive performance was significantly enhanced. The reason is that the obtained intercalated nanostructure possess high porosity to provide high double-layer capacitance. Unfortunately, the mechanical property deteriorated dramatically due to the poor interface interaction between graphene and nanoparticles. In order to solve this problem, nanoparticles such as unfunctionalized few-walled carbon nanotubes [20] were employed to improve the mechanical property of graphene fiber through the strong physical interaction (such as van der Waals forces et al.). However, hydrophilicity problem persisted, which led to the poor absorbance of electrolytes into the electrode, thus limited the improvement of capacitive performance. To this issue, hydrophilic polymer such as PVA [16,21] has been used to improve the hydrophilicity and mechanical properties, simultaneously, which was attributed to the hydroxyl groups on PVA chains (hydroxyl group is hydrophilic and strongly interacted with rGO by hydrogen bond). Nevertheless, due to the insulated polymer chain coating on the rGO sheets and breaking the linkage of graphene sheets on the fiber axis direction, the electric conductivity reduced severely, which in return significantly reduced the rate performance of device [16,22]. Therefore, it is a huge challenge to enhance the capacitive performance, mechanical property and hydrophilicity, simultaneously. Furthermore, under the condition that the conductivity is maintained at a high value.

Inspired by the advantages of different nanofillers reported above, an ideal nanofiller should possess lots of hydrophilic groups to improve the hydrophilicity and interface interaction of fiber. Moreover, the dimension of the nanofiller must be appropriate to restrain the π-π stacking of graphene nanosheets, but avoid to cause the non-linkage of graphene sheets. Cellulose nanocrystal (CNC) is typically formed of a rigid rod-like monocrystalline domain, 1–100 nm in diameter and hundreds of nanometers in length, which can be obtained from many cellulose materials by various simple methods [23–26]. In addition, this material has abundant hydroxyl groups on its surface. Thus the CNC entirely conforms to the requirements of expected nanofiller.

In this work, high performance rGO/CNC hybrid fibers were obtained from GO/CNC dispersion through non-liquid-crystal spinning, and then followed by chemical reduction. The results showed that their capacitive performance apparently enhanced, with mechanical properties and hydrophilicity simultaneously improved. Furthermore, the conductivity of hybrid fibers only reduced slightly. Moreover, the all-solid-state supercapacitors assembled from the as-prepared rGO/CNC-20 fiber exhibited a high specific capacitance of 123.2 F g^{-1} (155.8 F cm^{-3}) at a current density of 0.1 A g^{-1} (0.126 A cm^{-3}), good cycling stability, excellent flexibility and bending stability, high energy density (up to 5.1 mW h cm^{-3}) and power density (up to 496.4 mW cm^{-3}).

2. Experimental section

2.1. Materials

Graphite (F2) was obtained from Shanghai Yifan Graphite Co., Ltd. $KMnO_4$, $NaNO_3$, H_2O_2 (30%) and HI (45%) were purchased from Sinopharm Chemical Reagent Co., Ltd. H_2SO_4, CH_3COOH were purchased from Kunshan crystal microelectronics materials Co., Ltd. Polyvinyl alcohol (PVA) was acquired from Sinopec Shanghai Petrochemical Co., Ltd. Cellulose nanocrystal (CNC) was supplied by Guilin Qihong Technology Co., Ltd. and the CNC was purified by washing with deionized water and centrifuging (Centrifuge 5804R, Eppendorf, Germany; 10000r/min for 1 h to obtain CNC sediment), repeatedly (3 times). Finally, the purified CNC powder was obtained by lyophilization (LyoQuest-85, Telstar, Spain)

2.2. Preparation of the rGO and rGO/CNC hybrid fibers

Graphite Oxide (GO) was prepared from graphite by Hummer' method we reported previously [12,14,17]. 1 wt.% of GO dispersion was prepared by adding 4 g GO into 396 g deionized water and exfoliating with a digital ultrasonic processor (S-450D, Branson) for 2 h. Then the obtained GO dispersion was strongly stirred under a water bath at 60 °C, and was evaporated until a 2 wt.% GO dispersion was obtained. Next, the GO dispersion was mixed with CNC at different GO/CNC weight ratios of 100/0, 100/10, 100/20, 100/30 and 100/40, followed by sonication for 15 min to get uniform spinning dispersions.

GO and GO/CNC hybrid fibers were obtained by a novel non-liquid-crystal spinning we reported before [12,17]. For the non-liquid-crystal spinning processing, the jet stretch ratio used in this work was at 1.0. and the dispersions were injected into a rotating acetic acid bath by using a 10-mL syringe through a 23 G needle (330 μm in diameter) at a speed of 1.5 m min^{-1}. The coagulated wet fiber was immediately drawn out of the bath, and dried by a vertically-positioned infrared heater, then winded onto a polyethylene pipe. All the GO and GO/CNC hybrid fibers were reduced by immersing the fibers into HI solution at 85 °C for 8 h, then repeatedly washed by water and ethanol for three times. Finally dried at 60 °C in a vacuum. The obtained rGO fiber and rGO/CNC hybrid fibers were designated as rGO fiber, rGO/CNC-10 fiber, rGO/CNC-20 fiber, rGO/CNC-30 fiber and rGO/CNC-40 fiber. Pre-spinning dispersions with different components are shown in Table 1.

2.3. Assembly of the flexible all-solid-state supercapacitor

The PVA/H_2SO_4 gel electrolyte was prepared by adding 1 g PVA into 10 mL deionized water followed with magnetic stirring under 95 °C to get a uniform solution. After cooling to the room-temperature, 1 g of H_2SO_4 was added to the PVA solution under stirring to get the homogeneous PVA/H_2SO_4 gel electrolyte.

A rGO/CNC fiber-based all-solid-state supercapacitor was assembled by the method as we reported before [14,17]: Two rGO/CNC-20 fiber-based electrodes (each electrode consisted of five hybrid fibers) were immersed in the above PVA/H_2SO_4 gel electrolyte for 24 h, then drawn out and dried at room-temperature until the gel electrolyte solidified. The gelled electrodes were then arranged in parallel on a PET film, and the PVA/H_2SO_4 gel electrolyte was added to the empty space between the two gelled electrodes. After the gel electrolyte was dry, a scotch tape was pasted on the dried gel electrolyte to get the all-solid-state supercapacitor. In order to facilitate the test, pasting the ends of the two electrodes with copper wires by using silver paste was done.

2.4. Characterizations

The morphology of the GO sheet and the CNC was characterized using Atomic Force Microscope (AFM, NT-MDT, Prima) and Transmission Electron Microscope (TEM, JEOL, Japan). Polarized Optical

Table 1
Spinning dispersions with different components for neat rGO and rGO/CNC hybrid fiber fabricating.

Sample	GO (mg)	Deionized water (g)	CNC (mg)
rGO fiber	500.0	25.0	0.0
rGO/CNC-10 fiber	500.0	25.0	50.0
rGO/CNC-20 fiber	500.0	25.0	100.0
rGO/CNC-30 fiber	500.0	25.0	150.0
rGO/CNC-40 fiber	500.0	25.0	200.0

Microscope (POM) images of the GO/CNC and non-liquid-crystal GO/CNC dispersions were carried out by Alphaphot-2 optical microscope (Nikon, Japan). The rheological behavior of GO, GO/CNC and non-liquid-crystal GO/CNC dispersions were tested by ARES-RFS rheometer (TA Instruments, USA) using parallel plate geometry (50 mm diameter) with a gap of 8 ± 0.1 mm at 25 °C. The morphology of the rGO fiber and the rGO/CNC hybrid fibers were carried out by an SU8010 Filed-Emission Scanning Electron Microscope (FE-SEM, Hitachi, Japan). The average cross-sectional area of fibers was analyzed from the FE-SEM images by Image-Pro Plus software as previously demonstrated in our work [12,17]. The Fourier transform infrared (FTIR) spectra of CNC, GO fiber, rGO fiber, GO/CNC-20 fiber and rGO/CNC-20 fiber was obtained using a Nicolet NEXUS-670 spectrometer (Thermo Scientific, USA). The X-ray diffraction (XRD) spectra of the raw material and hybrid fibers were collected on a D/max 2550 PC diffractometer (Rigaku, Japan) with a Cu Kα radiation. The X-ray photoelectron spectra (XPS) of all the rGO and rGO/CNC hybrid fiber were collected on an Axis Ultra DLD spectrometer (Thermo ESCALAB 250, USA) using a monochromatic Al Ka source. The linear density of the fibers was calculated by dividing the mass of a filament with length (~3 m), where the mass was obtained from an XS microbalance (Mettler Toledo, USA, accurate of up to 0.00001).

The mechanical property of the fibers was tested on an XQ-1A fiber tension tester (Shanghai New Fiber Instrument, China): The gauge length was 10 mm and the extension rate was 2 mm min^{-1}. The electrical resistance of the fibers with a uniform length of 1.5 cm was tested on a multimeter (HEITHLEY 2000). At least 5 filaments of each fiber were tested for mechanical and resistance test, and average values of strength, modulus, elongation and electrical conductivity were calculated based on the average cross-sectional area of the fibers. The contact angle of the fibers was measured by optical contact angle measuring system (OCA 40 Micro, DataPhysics, Germany), and the pictures were taken immediately when deionized water droplet (about 50 nL) was dispensed onto the surface of fibers by a high-speed camera.

The tests of Cyclic Voltammetry (CV, from −0.6 V to 0.55 V at scan rates range from 2 to 100 mV s^{-1}), Galvanostatic Charge/Discharge (GCD) cycling (current densities from 0.2 to 2 A g^{-1}) and Electrochemical Impedance Spectroscopy (EIS, AC amplitude of 5 mV, frequencies between 10 mHz and 1 MHz) of the fibers were standard tested on CHI 660E electrochemical workstation (Shanghai Chenhua). The fiber electrode was prepared by connecting two segments of the same fiber to stainless-steel wire end by end with silver paste. Electrochemical tests were performed using a three-electrode configuration in 1 M H_2SO_4 electrolyte. Fiber electrode was used as the working electrode, Pt wire and Hg/Hg_2SO_4 electrode were used as the counter and reference electrodes, respectively. The silver paste was about 1 mm higher than the electrolyte surface and the immersion length of the fibers was ~1.3 cm. The CV and GCD cycling tests were also performed for the as prepared flexible all-solid-state supercapacitors, which were run from 0 V to 1 V with a scan rate ranging from 2 to 50 mV s^{-1} and a current density of 0.1–2 A g^{-1}, respectively.

The specific capacitance of the fibers (based on single electrode) was calculated from discharge part of CV and GCD curves by using $C = n(\int |I|dU)/v\triangle U$ and $C = nIT_d/(\triangle U\text{-}IR)$, where I represent the current, U is the potential, v represent the scan rate, $\triangle U$ represent the potential window, IR is the potential drop, T_d is the discharge time. The mass- and volume-specific capacitance were calculated based on the mass and the volume of the fiber electrode. The mass based energy density (E_M) and power density (P_M) of the supercapacitor were calculated from GCD curve (discharge part) by the equations as follows: $E_M = IT_d(\triangle U\text{-}IR)/4M$ and $P_M = I(\triangle U\text{-}IR)/4M$, respectively. And the values of energy density and power density based on volume was obtained by converting M to V.

3. Results and discussions

The morphologies of GO and CNC are shown in Fig. 1a and b. TEM image (Fig. 1a) shows the size of CNC nano-rod with ~300 nm in length and 20–30 nm in width. AFM image (Fig. 1b) indicates that GO nanosheets had a size of 500–1000 nm in width and a thickness of around 1.1–1.2 nm, which confirmed the efficient exfoliation of graphite by Hummer's method. Fig. 1c shows the results of the rheological test, it can be seen, that the viscosity of liquid-crystal GO/CNC dispersion was higher than liquid-crystal GO dispersion, and after adding NaOH, the viscosity of non-liquid-crystal GO/CNC dispersion was significantly decreased. In order to study this phenomenon, POM tests were carried out, and the POM images in Fig. 1d and e showed that the liquid-crystal GO/CNC-20 exhibited a vivid color with clumped distribution and formed an immobile gel (picture inset in Fig. 1d), indicating that the dispersion comprised of many large aggregates of liquid-crystal phase. As a contrast, no aggregate was found in the POM image of non-liquid-crystal GO/CNC dispersion, and it shows an easy flowing property (picture inset in Fig. 1e). Such phenomena was illustrated with the help of a diagram showing the formation and destruction of hydrogen bond (Fig. 1f): For liquid-crystal GO/CNC, there could form a strong hydrogen bonding network between CNC and GO, thus causing a higher viscosity than GO dispersion. After adding NaOH, the alkaline non-liquid-crystal suspension comprising of much higher negative charges on GO sheets, causing a stronger electrostatic repulsion between GO sheets and CNC, thus leading to the weaker hydrogen-bond interaction [27]. During spinning, the lower viscosity is predicted to favor the smooth extrusion of the non-liquid-crystal GO/CNC dispersion and shear-induced alignment of GO sheets. Furthermore, this homogeneous and easy flowing GO/CNC dispersion could also keep the continuous spinning of GO/CNC fibers [17]. Equipment for fabricating rGO and rGO/CNC hybrid fibers was simply shown in Fig. S1, which consists of extrusion unit, rotating acetic acid bath, IR heater and a winder. As Fig. 1g elaborates, continuous neat rGO and rGO/CNC hybrid fibers were successfully obtained via non-liquid-crystal spinning followed by HI reduction. First, the non-liquid-crystal dispersion was injected into the coagulating bath of acetic acid. During this process, water in extruded flow would be absorbed out by the acetic acid, and acetic acid would diffuse into the wet fiber. Furthermore, acetic acid can ionize with water and release protons to inhibit the dissociation of acidic groups on GO sheets, thus hydrogen bonding networks between the GO sheets and CNC would be reconstructed [12]. As a result, GO sheets and CNC could be coagulated through strong hydrogen-bond interaction. After drying under an IR heater and chemical reduction with HI, rGO and rGO/CNC hybrid fibers were then obtained. The high magnification FE-SEM image (inset green circle in Fig. 1g) of the cross-section of rGO/CNC shows that the CNC was uniformly dispersed within the hybrid fiber.

The cross-section morphology and summary on the parameters of the neat and hybrid fibers are shown in Fig. 2, and Table 2, respectively. It can be seen in Fig. 2a, that the neat rGO fiber shows a thin curvy belt-like cross-section with relatively disordered stacked rGO sheets. On the contrary, with the increasing of CNC content, the rGO/CNC hybrid fiber presented a cross-section (Fig. 2b–e) with thicker arms/walls and more ordered rGO sheets. It was also found out that the rGO/CNC hybrid fibers exhibited looser stacking of rGO sheets compared to neat rGO fiber. These differences between neat rGO fiber and rGO/CNC hybrid fibers all clearly originated from the contribution of CNC. On the one hand, owing to the inherent shape, size and hydrophilicity, CNC could work as efficient spacers and

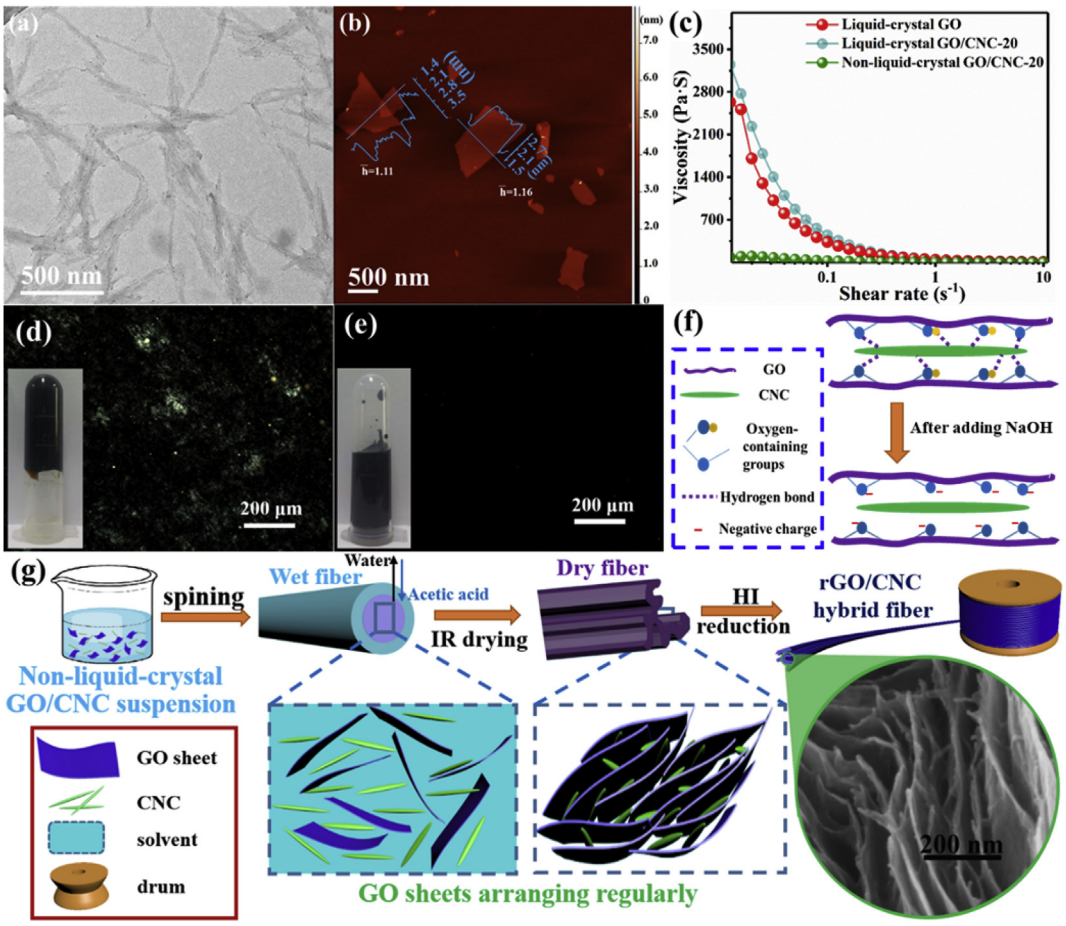

Fig. 1. (a) TEM image of CNC. (b) AFM image of GO. (c) Dependence of the viscosity of liquid-crystal and non-liquid-crystal dispersion on the shear rate. POM images of (d) liquid-crystal and (e) non-liquid-crystal GO/CNC-20 dispersion. (f) Diagram of the formation and destruction of hydrogen bond (g) Schematic illustration for the fabrication of rGO/CNC hybrid fiber. (A colour version of this figure can be viewed online.)

chemical absorbent for acetic acid. Thus, provided lots of nanochannels for acetic acid and water diffusion, causing a cross-section with thicker arms/walls [12] and prevent the stacking of GO sheets effectively. On the other hand, benefit from the rigid rod-like structure, CNC inhibited the curve or fold of GO sheets at nanoscale during the fiber formation in coagulating bath. Thus leading to a more ordered GO sheets, a similar phenomenon was also found in GO-NFC hybrid microfiber [26], and c (GO + NFC) microfiber [28]. After reduction with HI solution, rGO and rGO/CNC fibers were obtained and inherited most of the characteristics of their precursor fibers [12,17]. This orderly and loose structure of rGO sheets inside of the hybrid fibers could provide unobstructed channels for the diffusion of electrolyte ion.

Fig. 3a is the XRD pattern of raw materials and obtained fibers. GO powder showed a high intensity diffraction peak at 10.5° with no visible peak at 26°, indicating the successful oxidation and exfoliation of graphite [29]. The diffraction peak at around 23.9° of all the neat and hybrid fibers is ascribed to the graphite-like structure (002) face in graphene [17,30], which to some extent confirms the effective HI reduction. Meanwhile, the diffraction peaks at 14.9°, 16.5°, 22.8° belong to the $(1\bar{1}0)$, (110) and (200) plane of CNC, respectively [22–24]. With the increasing CNC contents, the intensity of CNC's diffraction peaks was increased. This confirmed that CNC was uniformly distributed in the hybrid fiber and therefore not hydrolyzed after HI reduction. The reason may be due to the high crystallinity of CNC and thus could readily resist the diffusion of H^+ into the CNC. Therefore, HI played an important role as a reductant when the GO and CNC existed side by side. The C 1s XPS spectra of raw materials and the obtained fibers (Fig. 3b) showed that the GO/CNC hybrid fiber (i.e., GO/CNC-20 fiber) has lots of oxygen-containing groups, such as hydroxyl/ether (286.3 eV-288.2 eV) and carbonyl/carboxyl groups (288.2 eV-290.3 eV). After reduction by HI solution, the intensity of hydroxyl/ether/epoxy groups became very weak, which proves an efficient reduction by HI [14,17,31]. The FTIR spectra (Fig. 3c) of rGO and rGO/CNC-20 fiber showed a weaker peak for C=O stretch (1720 cm^{-1}) than GO and GO/CNC-20 fiber, which is also attributed to the efficient reduction of HI. Also, easily note that the peak at 1200-1000 cm^{-1} (related to C–O stretch) of rGO and rGO/CNC-20 fiber became clearly higher than the counterpart in GO and GO/CNC-20 fiber. This could be ascribed to the side reaction of etherification happened between hydroxyl groups of GO and CNC, as a result provided a much strong interface interaction [12].

It is well known that excellent mechanical properties are essential requirements for candidate fibers to be used in self-supporting flexible electrodes. Fig. 4 shows the mechanical properties of the neat rGO and rGO/CNC hybrid fibers. Clearly, the strength of rGO and rGO/CNC hybrid fibers improved from 157.5 MPa to 230.6 MPa (enhanced by 46.4%) with the CNC content increased from 10% to 40%. The improvements are ascribed to the combination of the homogeneous dispersion of CNC in the graphene matrix and the improved interfacial interaction (hydrogen

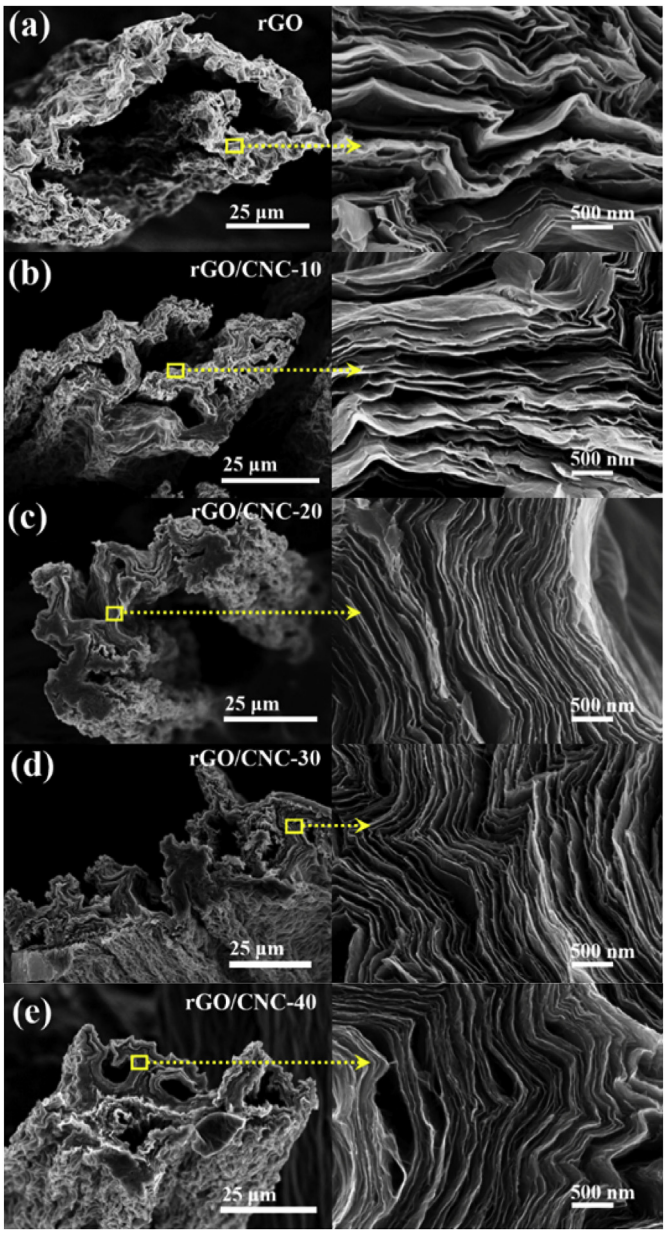

Fig. 2. Cross-section FE-SEM images of the rGO (a). rGO/CNC-10 (b). rGO/CNC-20 (c). rGO/CNC-30. (d) and rGO/CNC-40 (e). (A colour version of this figure can be viewed online.)

Table 2
Summary on the parameters of the rGO and rGO/CNC hybrid fibers.

Samples	Cross-sectional area (μm^2)	Linear density ($\mu g\ cm^{-1}$)
rGO fiber	792.7 ± 17.5	10.9
rGO/CNC-10 fiber	841.3 ± 9.6	11.8
rGO/CNC-20 fiber	850.9 ± 14.6	12.9
rGO/CNC-30 fiber	885.5 ± 18.7	13.3
rGO/CNC-40 fiber	913.9 ± 15.6	14.9

bonds and ether bonds between CNC and rGO) as revealed by XRD and FTIR analyses, respectively. But when the CNC content increased to 100%, the tensile strength decreased as shown in Fig. S2, which could be due to the reason that the more CNC content would increase the gap between adjacent graphene sheets, thus weaken the π-π bond, and leading to the decrease of the mechanical properties [42]. While the elongation at break decreased from 6.2% to 4.3%, the modulus increased from 4.29 GPa to 6.51 GPa. Similar results were also been reported for GO-NFC hybrid microfiber [26]. Which is attributed to the CNC acting as an efficient spacer to avoid the restacking of rGO sheets, and the strong interfacial interaction causing more difficult slide and shear of the laminated structure under a certain strain. When the CNC content reached a high value (about 30 wt.%), the difficulty in sliding and shearing reached to the highest, which therefore led to a slight change in elongation and modulus of hybrid fibers. However, the elongation still had the typical value of about 3–6% for graphene based fibers, which is comparable to that of CNT fibers, and much higher than graphite fibers (about 1%) [10]. More importantly, the tensile strength of hybrid fiber reported in here is stronger than the SWNT/rGO hybrid fiber-2 (123 MPa) [1], MnO_2/rGO-20 fiber (93 MPa) [14], and nacre-mimicking CRG@PVA fibers (161 MPa) [21]. This suggests that the CNC effectively improved the mechanical properties of graphene fiber, and the resultant rGO/CNC hybrid fibers can easily meet the application requirement of flexible or even wearable supercapacitor.

Owing to the reason known to all, the hydrophilic nature of the electrode readily facilitates the penetration of electrolyte. In this line, therefore, it is crucial to ameliorate the affinity of graphene based electrodes for improving their electrochemical performance [9,12,17]. Fig. 5a shows the contact angle of neat rGO and rGO/CNC hybrid fibers. Same as rGO fiber prepared by our group previously [12,17], the rGO fiber presented the typical hydrophobicity with a water contact angle of 105.7°. On the contrary, with the CNC content increasing from 10 wt.% to 40 wt.%, the contact angle gradually decreased to 85.6°, 63.3°, 51.8° and 40.5°, indicating an improved hydrophilicity of rGO/CNC hybrid fibers. This obvious improvement in the hydrophilicity was associated with the introduction of CNC. On the one hand, hydrophilic CNC could improve the hydrophilicity of rGO fiber. On the other hand, surface morphology was altered according to Table 2 (also shown in Fig. S3), thus could improve the hydrophilicity [40,41]. Combining with the orderly aligned rGO sheets (witnessed by FESEM earlier), it could provide an unhindered and hydrophilic nano-channel for facilitating the transport of electrolyte ions across the fiber.

An excellent electrical conductivity of the electrode in the supercapacitor would construct a fast electron transport network, leading to a good rate performance [14]. The conductivity of the neat rGO and rGO/CNC hybrid fibers is given in Fig. 5b. The conductivity only changed slightly from 71.9 S cm^{-1} for neat rGO fiber to 58.8 S cm^{-1} for rGO/CNC-40 fiber, indicating an excellent conductivity of both neat rGO and rGO/CNC hybrid fibers. The possible reason for the conductivity change of rGO/CNC hybrid fibers could be explained in two aspects: On the one hand, the CNC with a shape of nano-rod cannot form a coating on the rGO sheets, thus the linkage of rGO sheet edges in the direction of fiber axis would almost not break (as illustrated in the picture inset Fig. 5b), and the direct electron transport pathway still remained at high quality, which will have a major impact in the conductivity. On the other hand, after adding CNC, it would increase the layer spacing of rGO sheets, and thus decreased the electron hopping among rGO sheets, causing a minor decrease in conductivity [17]. It is worth noting that the effect of CNC is extremely different from that of amorphous polymer nanofillers such as PVA [17,21], Polyaniline [32]. By introducing the polymer to rGO, polymers tend to form a coating on the rGO sheets, therefore interfere with the linkage of rGO sheets in the direction of fiber axis, thus causing an apparent degradation on the conductivity of the hybrid fibers compared to neat rGO fiber. Thus it can be concluded that the rGO/CNC hybrid fibers showed a high conductivity which predicts excellent capacitive performance when applied as fiber electrode for energy storage applications.

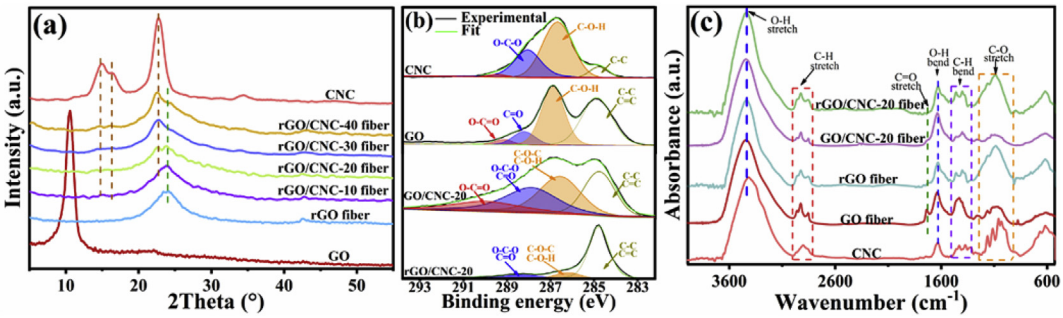

Fig. 3. (a) XRD spectra, (b) C 1s XPS core level spectra and (c) FTIR spectra of the raw materials and obtained fibers. (A colour version of this figure can be viewed online.)

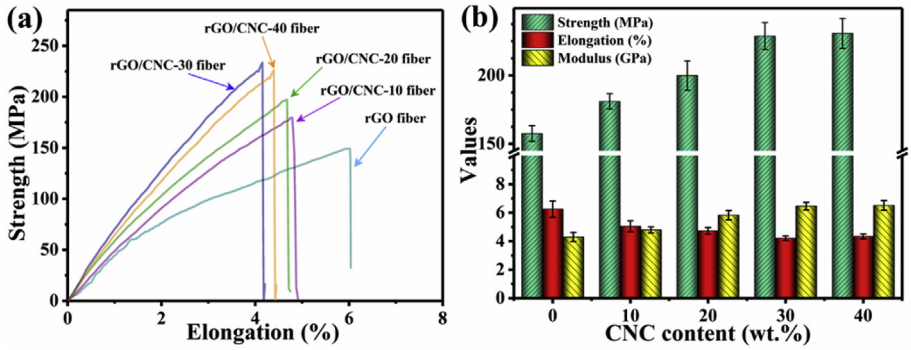

Fig. 4. Mechanical properties of the neat rGO and rGO/CNC hybrid fibers. (a) Typical tensile stress-strain curves. (b) Strength, elongation and modulus dependent on the CNC content. (A colour version of this figure can be viewed online.)

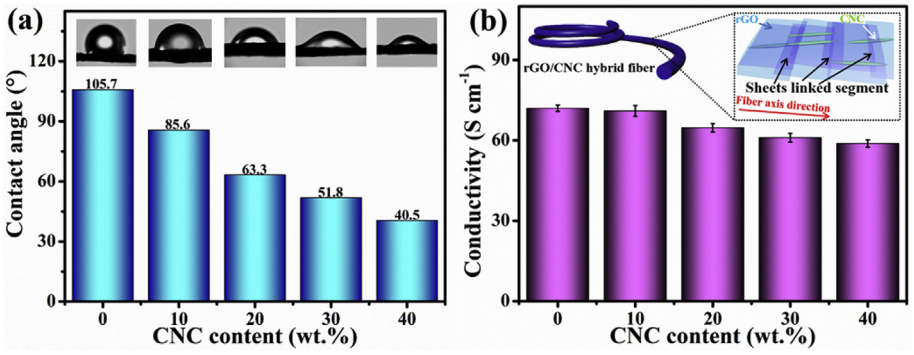

Fig. 5. Contact angle (a) and conductivity (b) of neat rGO and rGO/CNC hybrid fibers. (A colour version of this figure can be viewed online.)

The electrochemical test results of neat rGO and rGO/CNC hybrid fibers are shown in Fig. 6. In order to optimize the operational voltage window of electrodes, we tested the CV curves under different scan rate as shown in Fig. S4, we found out that when using the voltage window of −0.6 to 0.55 or −0.6 to 0.7, obvious peaks surfaced caused by the oxygen reduction. So we used the voltage window of −0.6 to 0.4, which almost showed no peak caused by the oxygen reduction. For the CV test at the scan rate of 10 mV s^{-1} (Fig. 7a), the curve with low area of the rGO fiber indicated a mass-specific capacitance of only 5.0 F g^{-1}. On the contrary, the curves of rGO/CNC hybrid fibers exhibited the distinct higher area, and reached the highest mass-specific capacitance of 121.2F g^{-1} at the CNC loading level of 20 wt.%. Furthermore, it can be seen that each CV curve of different sample shoed a pair of redox peaks, which was caused by the typical transition between quinone/hydroquinone groups on graphene sheets in 1 M H_2SO_4 [9,12,33], which was corresponding to the C═O peak in XPS spectra in Fig. S5. Fig. 6b shows the mass-specific capacitance of rGO fiber and rGO/CNC hybrid fibers with the increasing CNC content at the different scan rate. As the CNC content increased, the specific capacitance tends to increase first, then decrease and achieving the highest mass-specific capacitance at the CNC content of 20 wt.%. The reason for this can be summarized in two aspects: Firstly, the improved hydrophilicity and orderly aligned rGO sheets of hybrid fibers facilitated the absorption and diffusion of electrolyte ions across the fiber. Secondly, the spacer effect which caused looser restacking of rGO sheets is thought to offer a dramatically higher inner surface area (supplied in Fig. S6), and thus more oxygen containing groups were exposed and more electrolyte ions were possibly absorbed into the fiber. However, extra loading of CNC could fill the gaps and leave less room for the ion diffusion through the fiber, thus lesser electrical double-layer capacitor and faradic capacitance leading to

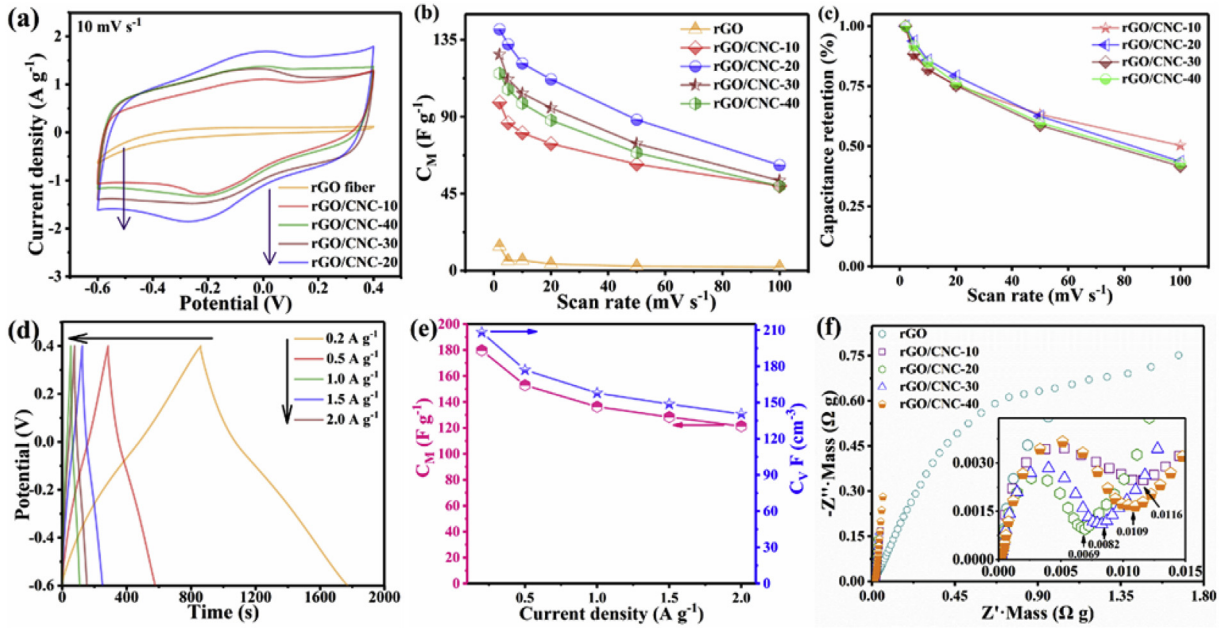

Fig. 6. Electrochemical properties of the rGO fiber and rGO/CNC hybrid fibers. (a) CV curves at 10 mV s^{-1}. (b) Specific capacitance at different scan rates. (c) The capacitance retention ratio based on the scan rates. (d) GCD curves of rGO/CNC-20 fiber at different current density. (e) Specific capacitance at a different current density of rGO/CNC-20 fiber. (f) EIS of all the fibers. (A colour version of this figure can be viewed online.)

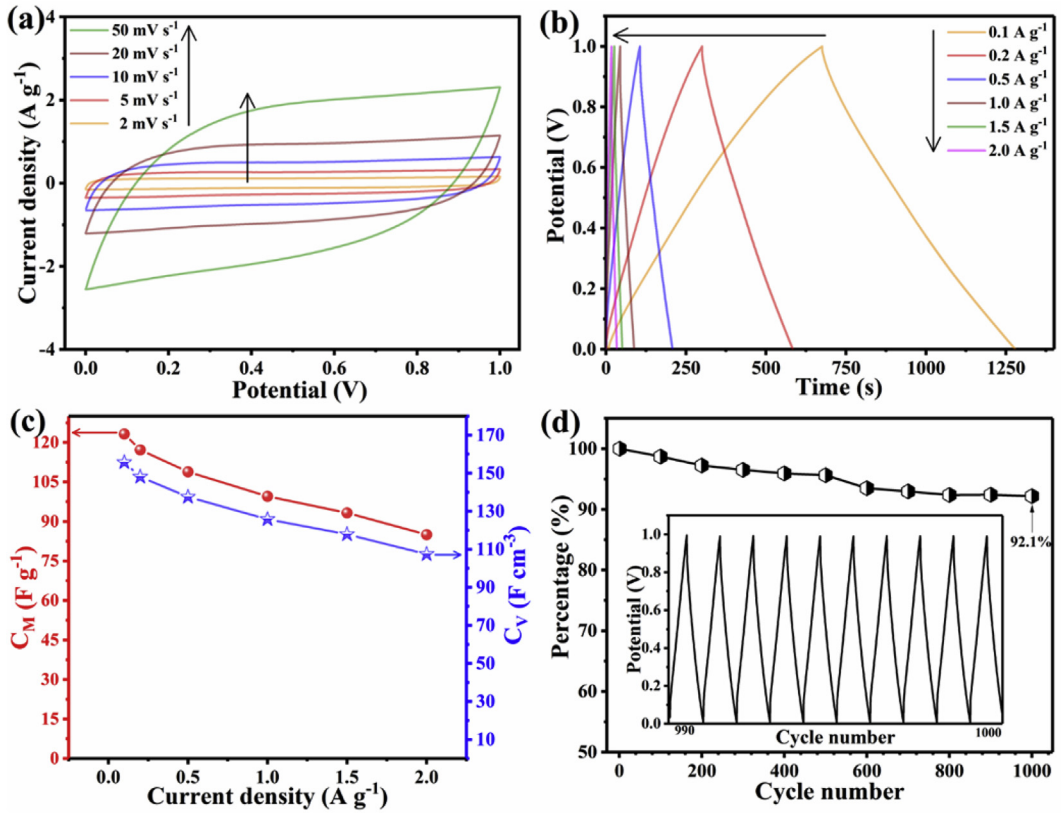

Fig. 7. Electrochemical performance of all-solid-state supercapacitor assembled from the rGO/CNC-20 fibers. (a) CV curves at different scan rates. (b) GCD curves at different current density. (c) Volume- and mass-specific capacitance at different current densities. (d) Change of the capacitance ratio during the GCD cycling at 1.0 A g^{-1}. (A colour version of this figure can be viewed online.)

the decrease in mass-specific capacitance of rGO/CNC hybrid fibers. Fig. 6c shows the capacitance retention ratio based on the different scan rates, it can be found that all the rGO/CNC hybrid fibers showed a high capacitance retention ratio (within 58%–63%) at

high scan rate (50 mV s^{-1}), which is further significantly improved based on our work previously (PVA/rGO hybrid fiber [17], of about 23% at 50 mV s^{-1}). As well as, the CV test results showed that the rGO/CNC-20 fiber had the highest mass-specific capacitance of 141.1 F g^{-1} and 132.3 F g^{-1} at scan rate of 2 mV s^{-1} and 5 mV s^{-1} respectively. This value of mass-specific capacitance is much higher than CNFs (105.4 F g^{-1} at 5 mV s^{-1}, in 2 M KOH) [7], rGO/CB-1.5 film (95.7 F g^{-1} at 5 mV s^{-1}, in 1 M H_2SO_4) [22] and CNT-coated carbon fiber (~11 F g^{-1} at 2 mV s^{-1}, in 1 M H_2SO_4) [34]. Fig. 6d and e shows the GCD curves and the specific capacitance of rGO and rGO/CNC hybrid fibers at the different current density, it can be seen that a specific capacitance value as high as 179.7 F g^{-1} (208.2 F cm^{-3}) was achieved at a current density of 0.2 A g^{-1} (0.251 A cm^{-3}), which is comparable to that of DEG/graphene (194.5 F g^{-1} at current density of 0.2 A g^{-1}, in 6 M KOH solution) [16]. Moreover, it is worth noting that all the rGO/CNC hybrid fibers exhibited excellent rate performance. For example, rGO/CNC-20 fiber showed a specific capacitance of 121.3 F g^{-1} (140.5 F cm^{-3}) at the current density of 2.0 A g^{-1} (2.51 A cm^{-3}) due to the high conductivity and the unobstructed channels for the diffusion of electrolyte ion.

EIS can provide information about ion transmission and electrochemical properties of both electrode and electrolytes. Results of EIS measurement are shown in Fig. 6f, it can be seen in lower frequency range, the plots for all rGO/CNC hybrid fibers are nearly vertical to the Z' axis. As a contrast, the plot of rGO was more inclined, implying rGO/CNC hybrid fibers could provide better nanochannels for ions diffusion [35] due to the CNC being able to act as efficient spacers and the improved hydrophilicity. This result and its explanation are consistent with the FE-SEM and contact angle results. Furthermore, the charge transfer resistance (the diameter of the semicircle) decreased in the order of rGO fiber, rGO/CNC-10 fiber, rGO/CNC-40 fiber, rGO/CNC-30 fiber and rGO/CNC-20 fiber, indicating that the rGO/CNC-20 fiber with the most appropriate CNC loading level, demonstrating the best electrochemical performance.

An all-solid-state supercapacitor was assembled from two bundles (five fibers every bundle) of rGO/CNC-20 hybrid fiber onto the substrate of PET film. The CV test of this device was carried out, and the result (Fig. 7a) shows the device had a quasi-rectangular curves at the low scan rate (2–20 mV s^{-1}), and still remain a relatively rectangular shape without obvious distortion at the scan rate of 50 mV s^{-1}, indicating the desirable fast charge and discharge property. Fig. 7b shows the GCD curves of this device, the resultant GCD curves were nearly triangular with low potential drop region at different current densities, demonstrating a good charge transportation across the fibers. The variation of device volume- or mass-specific capacitance at different current densities based on the GCD curves are shown in Fig. 7c. The device demonstrated a high specific capacitance of 123.3 F g^{-1} (155.8 F cm^{-3}) and 117.2 F g^{-1} (148.1 F cm^{-3}) at the current density of 0.1 A g^{-1} (0.126 A cm^{-3}) and 0.2 A g^{-1} (0.251 A cm^{-3}), respectively. These capacitance values are much higher than those of CNT_1-RGO_4 WSS (32.5 F cm^{-3}, at 0.3 A cm^{-3}) [20], RGO core-sheath fiber (~38 F g^{-1} at 0.2 A g^{-1}) [36], and rGO–MoS_2 (2.2 wt%) hybrid fiber (~27 F cm^{-3} at 0.2 A cm^{-3}) [37] based devices. Furthermore, it is worth noting that when the current density is increased, the specific capacitance only reduced to 99.8 F g^{-1} (125.8 F cm^{-3}) at 1.0 A g^{-1}, and 85.0 F g^{-1} (107.4 F cm^{-3}) at 2.0 A g^{-1}, which related to a high capacitance retention rate of 81% and 69.0%, indicating an excellent capacitance performance during the fast charge-discharge process. This can be ascribed to the relatively high conductivity after introducing the CNC. Fig. 7d shows the cycling stability of the device, which was evaluated by cyclic GCD tests at 1.0 A g^{-1}. The result shows that after charge and discharge for 1000 cycles, its specific capacitance was still kept at 92.1%. This capacitance loss (about 7.9%) was also reported for many kinds of rGO based fibers [17].

For further applications, supercapacitors usually need to be connected in series or parallel to fit in different currents and operating voltages. Fig. 8a shows the GCD curves of three devices connected in parallel or series compared to single one. The discharge time of three devices connected in parallel is nearly three times than that of single device. And under the similar discharge time, the voltage window can be elevated from 1.0 V for a single device to 3.0 V by connecting three devices in series. In order to evaluate the flexibility of the device, GCD curves under different bending angles (0°, 45°, 90°, 135°, 180°, in accordance with the pictures inset in Fig. 8b) and different bending times were measured, Fig. 8b shows the bending stability of the device. It indicates that the capacitance remained nearly 100% under different bending angles, and a 97.2% retention ratio is observed after bending at 180° for 500 times, indicating an excellent flexibility and bending stability of this device. These results demonstrate that the supercapacitor could act as an excellent energy storage device for flexible electronics. Fig. 8c shows the ragone plot of the volumetric energy and power density of the device compare with commercially available supercapacitors and other energy-storage systems. Our fabricated supercapacitor showed an energy density as high as 5.1 mW h cm^{-3} at the power density of 30.7 mW cm^{-3}. This values are higher than the 5.5 V/100 mF commercial supercapacitor (0.55 mW h cm^{-3} at 9 mW cm^{-3}) and 2.75 V/44 mF commercial supercapacitor (0.7 mW h cm^{-3} at 590 mW cm^{-3}) [14,17]. Compared to Li thin film battery [38], our supercapacitor had a much higher power density and closely energy density. Moreover, this energy density value is also higher than that of various graphene and carbon fiber-based supercapacitors such as rGO-MoS_2 supercapacitor (4.15 mW h cm^{-3} at 21 mW cm^{-3}) [37], MnO_2

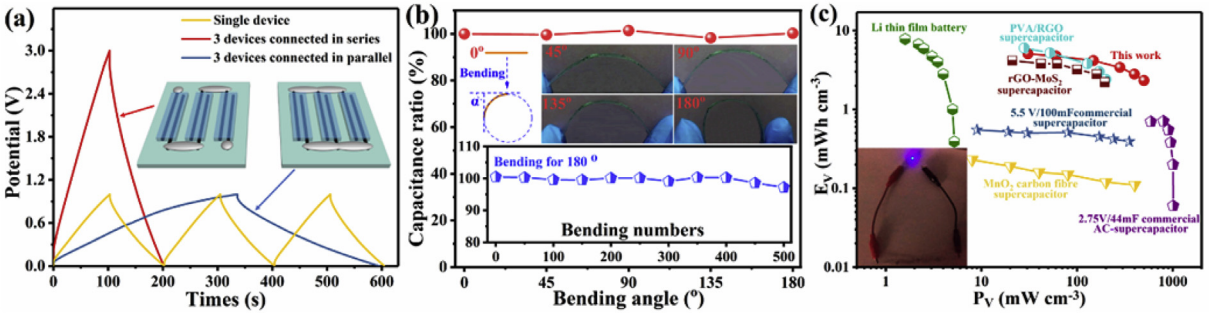

Fig. 8. (a) GCD curves of single and three devices connected in parallel and series. (b) Bending stability of the device. (c) Comparison of volumetric energy and power densities of the device with commercially supercapacitors and other energy-storage systems: PVA/RGO SC [16], rGO-MoS_2 SC [37], Li thin film battery [38] and MnO_2 carbon fiber SC [39]. (A colour version of this figure can be viewed online.)

carbon fiber supercapacitor (0.23 mW h cm^{-3} at 8 mW cm^{-3}) [39], and comparable to our previously works: a hierarchical MnO_2/RGO hybrid fiber-based supercapacitor (5.8 mW h cm^{-3}) [14] and PVA/RGO hybrid fiber-based supercapacitor (5.97 mW h cm^{-3}) [17]. We note that the power density of our fabricated supercapacitor reached to 496.4 mW cm^{-3}, which is much higher than Li thin film battery and comparable to 2.75 V/44 mF commercial supercapacitor and our work previously (a hierarchical MnO_2/RGO hybrid fiber-based supercapacitor) [14,38].

4. Conclusion

In summary, continuous rGO/CNC hybrid fibers were successfully fabricated via non-liquid-crystal spinning followed by chemical reduction. The results showed that the rGO/CNC hybrid fibers possessed an unobstructed nano-channels constructed of ordered loose rGO sheets, improved capacitive performance, exceptional mechanical properties, hydrophilicity, and high conductivity. Furthermore, as the optimized hybrid fiber, rGO/CNC-20 showed the highest specific capacitance (141.1 F g^{-1} at 2 mV s^{-1}), and an all-solid-state supercapacitor fabricated from this hybrid fiber exhibited a high specific capacitance (123.3 F g^{-1} or 155.8 F cm^{-3} at the current density of 0.1 A g^{-1}), excellent flexibility, outstanding cycling stability (92% capacitance retention over 1000 cycles), high energy density and power density (5.1 mWh cm^{-3} and 496.4 mW cm^{-3}, respectively). In addition, this work provides an efficient strategy to fabricate graphene based fiber-shaped electrodes with high capacitive performance, and simultaneously improved mechanical properties, hydrophilicity, meanwhile keep the conductivity at a high value owing to the nanoscale assembly of nanoparticles with the abundant hydrophilic groups on their surface.

Acknowledgements

This work was supported by the National Natural Science Foundation of China (51603038, 51673038), Program for Changjiang Scholars and Innovative Research Team in University (IRT16R13), Science and Technology Commission of Shanghai Municipality (16JC1400700), Innovation Program of Shanghai Municipal Education Commission (2017-01-07-00-03-E00055) and the Baoshan production and research project (16-C-12).

Appendix A. Supplementary data

Supplementary data related to this article can be found at https://doi.org/10.1016/j.carbon.2017.11.012.

References

[1] D.S. Yu, K.L. Goh, H. Wang, L. Wei, W.C. Jiang, Q. Zhang, et al., Scalable synthesis of hierarchically structured carbon nanotube-graphene fibres for capacitive energy storage, Nat. Nanotechnol. 9 (7) (2014) 555–562.
[2] Y.L. Shao, M.F. El-Kady, L.J. Wang, Q.H. Zhang, Y.G. Li, H.Z. Wang, Graphene-based materials for flexible supercapacitors, Chem. Soc. Rev. 44 (11) (2015) 3639–3665.
[3] N. Li, Z.P. Chen, W.C. Ren, F. Li, H.M. Cheng, Flexible graphene-based lithium ion batteries with ultrafast charge and discharge rates, Proc. Natl. Acad. Sci. U. S. A. 109 (43) (2012) 17360–17365.
[4] A. Ramadoss, K.Y. Yoon, M.J. Kwak, S.I. Kim, S.T. Ryu, J.H. Jang, Fully flexible, lightweight, high performance all-solid-state supercapacitor based on 3-dimensional-graphene/graphite-paper, J. Power Sources 337 (2017) 159–165.
[5] M. Sawangphruk, P. Srimuk, P. Chiochan, A. Krittayavathananon, S. Luanwuthi, J. Limtrakul, High-performance supercapacitor of manganese oxide/reduced graphene oxide nanocomposite coated on flexible carbon fiber paper, Carbon 60 (2013) 109–116.
[6] F.C. Meng, W.B. Lu, Q.W. Li, J.H. Byun, Y. Oh, T.W. Chou, Graphene-based fibers: a review, Adv. Mater. 27 (35) (2015) 5113–5131.
[7] W.D. Yu, W.R. Lin, X.F. Shao, Z.X. Hu, R.C. Li, D.S. Yuan, High performance supercapacitor based on Ni_3S_2/carbon nanofibers and carbon nanofibers electrodes derived from bacterial cellulose, J. Power Sources 272 (2014) 137–143.
[8] Z.X. Tai, X.B. Yan, J.W. Lang, Q.J. Xue, Enhancement of capacitance performance of flexible carbon nanofiber paper by adding graphene nanosheets, J. Power Sources 199 (2012) 373–378.
[9] Y. Chen, X. Zhang, D.C. Zhang, P. Yu, Y.W. Ma, High performance supercapacitors based on reduced graphene oxide in aqueous and ionic liquid electrolytes, Carbon 49 (2) (2011) 573–580.
[10] Z.L. Dong, C.C. Jiang, H.H. Cheng, Y. Zhao, G.Q. Shi, L. Jiang, et al., Facile fabrication of light, flexible and multifunctional graphene fibers, Adv. Mater. 24 (14) (2012) 1856–1861.
[11] L.B. Liu, Y. Yu, C.S. Yan, K. Li, Z.J. Zheng, Wearable energy-dense and power-dense supercapacitor yarns enabled by scalable graphene-metallic textile composite electrodes, Nat. Commun. 6 (2015) 7260.
[12] S.H. Chen, W.J. Ma, Y.H. Cheng, Z. Weng, B. Sun, L. Wang, et al., Scalable non-liquid-crystal spinning of locally aligned graphene fibers for high-performance wearable supercapacitors, Nano Energy 15 (2015) 642–653.
[13] Q. Chen, Y.N. Meng, C.G. Hu, Y. Zhao, H.B. Shao, N. Chen, et al., MnO_2-modified hierarchical graphene fiber electrochemical supercapacitor, J. Power Sources 247 (2014) 32–39.
[14] W.J. Ma, S.H. Chen, S.Y. Yang, W.P. Chen, Y.H. Cheng, Y.W. Guo, et al., Hierarchical MnO_2 nanowire/graphene hybrid fibers with excellent electrochemical performance for flexible solid-state supercapacitors, J. Power Sources 306 (2016) 481–488.
[15] H.J. Fei, C.Y. Yang, H. Bao, G.C. Wang, Flexible all-solid-state supercapacitors based on graphene/carbon black nanoparticle film electrodes and cross-linked poly (vinyl alcohol)-H_2SO_4 porous gel electrolytes, J. Power Sources 266 (2014) 488–495.
[16] Y. Yu, Y.B. Sun, C.Y. Cao, S.L. Yang, H. Liu, P. Li, et al., Graphene-based composite supercapacitor electrodes with diethylene glycol as inter-layer spacer, J. Mater. Chem. A 2 (21) (2014) 7706–7710.
[17] S.H. Chen, W.J. Ma, H.X. Xiang, Y.H. Cheng, S.Y. Yang, W. Weng, et al., Conductive, tough, hydrophilic poly(vinyl alcohol)/graphene hybrid fibers for wearable supercapacitors, J. Power Sources 319 (2016) 271–280.
[18] W.J. Ma, S.H. Chen, S.Y. Yang, W.P. Chen, W. Weng, Y.H. Cheng, et al., Flexible all-solid-state asymmetric supercapacitor based on transition metal oxide nanorods/reduced graphene oxide hybrid fibers with high energy density, Carbon 113 (2017) 151–158.
[19] L. Kou, T.Q. Huang, B.N. Zheng, Y. Han, X.L. Zhao, K. Gopalsamy, et al., Coaxial wet-spun yarn supercapacitors for high-energy density and safe wearable electronics, Nat. Commun. 5 (2014) 3754.
[20] Y.W. Ma, P. Li, J.W. Sedloff, X. Zhang, H.B. Zhang, J. Liu, Conductive graphene fibers for wire-shaped supercapacitors strengthened by unfunctionalized few-walled carbon nanotubes, ACS Nano 9 (2) (2015) 1352–1359.
[21] L. Kou, C. Gao, Bioinspired design and macroscopic assembly of poly (vinyl alcohol)-coated graphene into kilometers-long fibers, Nanoscale 5 (10) (2013) 4370–4378.
[22] Y.M. Wang, J.C. Chen, J.Y. Cao, Y. Liu, Y. Zhou, J.H. Ouyang, et al., Graphene/carbon black hybrid film for flexible and high rate performance supercapacitor, J. Power Sources 271 (2014) 269–277.
[23] J.P.F. Lagerwall, C. Schütz, M. Salajkova, J.H. Noh, J.H. Park, G. Scalia, et al., Cellulose nanocrystal-based materials: from liquid crystal self-assembly and glass formation to multifunctional thin films, NPG Asia Mater. 6 (2014) e80.
[24] H.L. Zhu, W. Luo, P.N. Ciesielski, Z.Q. Fang, J.Y. Zhu, G. Henriksson, et al., Wood-derived materials for green electronics, biological devices, and energy applications, Chem. Rev. 116 (16) (2016) 9305–9374.
[25] H.Y. Yu, B. Sun, D.Z. Zhang, G.Y. Chen, X.Y. Yang, J.M. Yao, Reinforcement of biodegradable poly (3-hydroxybutyrate-co-3-hydroxyvalerate) with cellulose nanocrystal/silver nanohybrids as bifunctional nanofillers, J. Mater. Chem. B 2 (48) (2014) 8479–8489.
[26] Y.Y. Li, H.L. Zhu, S.Z. Zhu, J.Y. Wan, Z. Liu, O. Vaaland, et al., Hybridizing wood cellulose and graphene oxide toward high-performance fibers, NPG Asia Mater. 7 (2015) e150.
[27] H. Bai, C. Li, X.L. Wang, G.G. Shi, A pH-sensitive graphene oxide composite hydrogel, Chem. Comm. 46 (14) (2010) 2376–2378.
[28] Y.Y. Li, H.L. Zhu, F. Shen, J.Y. Wan, X.G. Han, J.Q. Dai, et al., Highly conductive microfiber of graphene oxide templated carbonization of nanofibrillated cellulose, Adv. Funct. Mater. 24 (46) (2014) 7366–7372.
[29] L. Zhang, J.J. Liang, Y. Huang, Y.F. Ma, Y. Wang, Y.S. Chen, Size-controlled synthesis of graphene oxide sheets on a large scale using chemical exfoliation, Carbon 47 (14) (2009) 3365–3368.
[30] S.P. Zhou, H.M. Zhang, Q. Zhao, X.H. Wang, J. Li, F.S. Wang, Graphene-wrapped polyaniline nanofibers as electrode materials for organic supercapacitors, Carbon 52 (2013) 440–450.
[31] S.F. Pei, J.P. Zhao, J.H. Du, W.C. Ren, H.M. Cheng, Direct reduction of graphene oxide films into highly conductive and flexible graphene films by hydrohalic acids, Carbon 48 (15) (2010) 4466–4474.
[32] Z.X. Tai, X.B. Yan, Q.J. Xue, Three-dimensional graphene/polyaniline composite hydrogel as supercapacitor electrode, J. Electrochem. Soc. 159 (10) (2012) A1702–A1709.
[33] Y.J. Oh, J.J. Yoo, Y.I. Kim, J.K. Yoon, H.N. Yoon, J.H. Kim, et al., Oxygen functional groups and electrochemical capacitive behavior of incompletely reduced graphene oxides as a thin-film electrode of supercapacitor, Electrochim. Acta 116 (2014) 118–128.

[34] V.T. Le, H. Kim, A. Ghosh, J. Kim, J. Chang, Q.A. Vu, D.T. Pham, J.H. Lee, S.W. Kim, Y.H. Lee, Coaxial fiber supercapacitor using all-carbon material electrodes, ACS Nano 7 (7) (2013) 5940–5947.
[35] X.J. Wei, X.Q. Jiang, J.S. Wei, S.Y. Gao, Functional groups and pore size distribution do matter to hierarchically porous carbons as high-rate-performance supercapacitors, Chem. Mater. 28 (2) (2016) 445–458.
[36] Y.N. Meng, Y. Zhao, C.G. Hu, H.H. Cheng, Y. Hu, Z.P. Zhang, G.Q. Shi, L.T. Qu, All-graphene core-sheath microfibers for all-solid-state, stretchable fibriform supercapacitors and wearable electronic textiles, Adv. Mater. 25 (16) (2013) 2326–2331.
[37] G.Z. Sun, J.Q. Liu, X. Zhang, X.W. Wang, H. Li, Y. Yu, et al., Fabrication of ultralong hybrid microfibers from nanosheets of reduced graphene oxide and transition-metal dichalcogenides and their application as supercapacitors, Angew. Chem. Int. Ed. 53 (46) (2014) 12576–12580.
[38] D. Pech, M. Brunet, H. Durou, P. Huang, V. Mochalin, Y. Gogotsi, Pi.L. Taberna, P. Simon, Ultrahigh-power micrometre-sized supercapacitors based on onion-like carbon, Nat. Nanotechnol. 5 (9) (2010) 651–654.
[39] X. Xiao, T.Q. Li, P.H. Yang, Y. Gao, H.Y. Jin, W.J. Ni, et al., Fiber-based all-solid-state flexible supercapacitors for self-powered systems, ACS Nano 6 (10) (2012) 9200–9206.
[40] J. Zhu, C.M. Hsu, Z.F. Yu, S.H. Fan, Y. Cui, Nanodome solar cells with efficient light management and self-cleaning, Nano Lett. 10 (6) (2010) 1979–1984.
[41] K.H. Tsui, Q.F. Lin, H.T. Chou, Q.P. Zhang, H.Y. Fu, P.F. Qi, et al., Flexible, and self-cleaning 3D nanocone anti-reflection films for high-efficiency photovoltaics, Adv. Mater. 26 (18) (2014) 2805–2811.
[42] G.Q. Xin, T.K. Yao, H.T. Sun, S.M. Scott, D.L. Shao, G.K. Wang, et al., Highly thermally conductive and mechanically strong graphene fibers, Science 349 (6252) (2015) 1083.